Supplemental Material for "Structure from Motion of Multi-Angle RPAS Imagery Complements Larger-Scale Airborne Lidar Data for Cost-Effective Snow Monitoring in Mountain Forests"

Patrick D. Broxton, Willem J.D. van Leeuwen

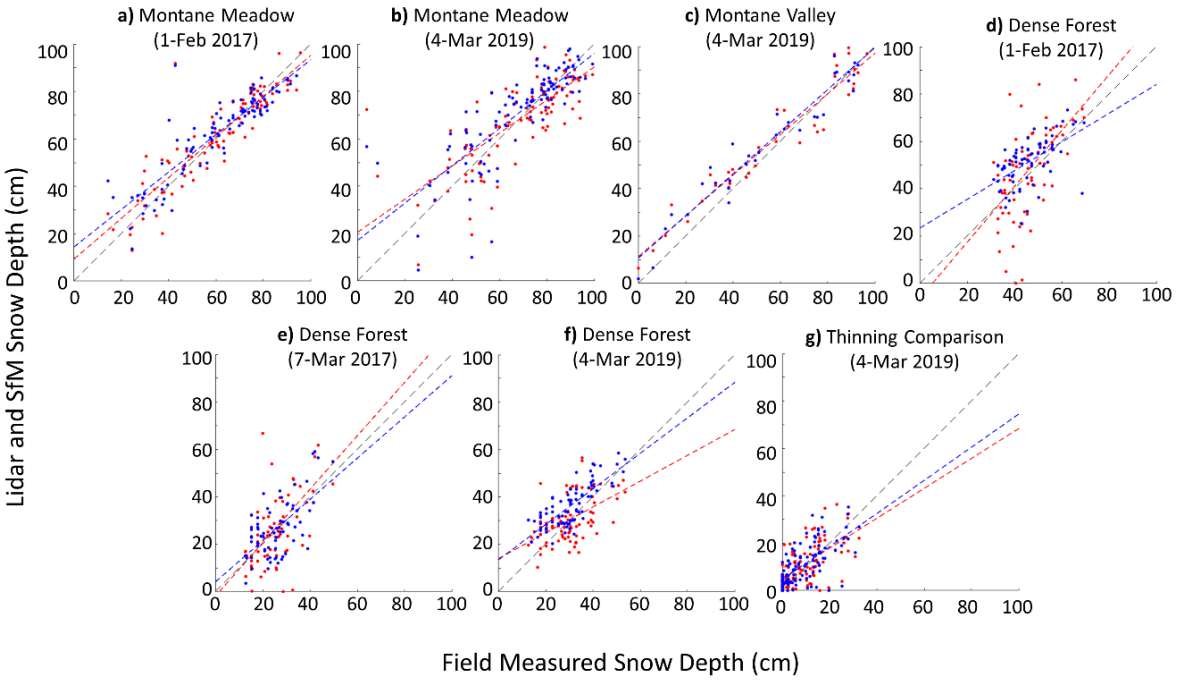

Figure S1. Scatterplots between the field measured snow depths and SfM (red dots) and lidar (blue dots) snow depth data for the paired manned aircraft lidar-UAS SfM surveys for the montane meadow plot on 1 February 2017 (**a**) and 4 March 2019 (**b**); the montane valley plot on 4 March 2019 (**c**); the dense forest on 1 February 2017 (**d**), 7 March 2017 (**e**), and 4 March 2019 (**f**); and thinning comparison plot on 4 March 2019 (**g**). The colored dotted lines show the best-fit linear regressions for each comparison, and the black dotted line is the 1:1 line.

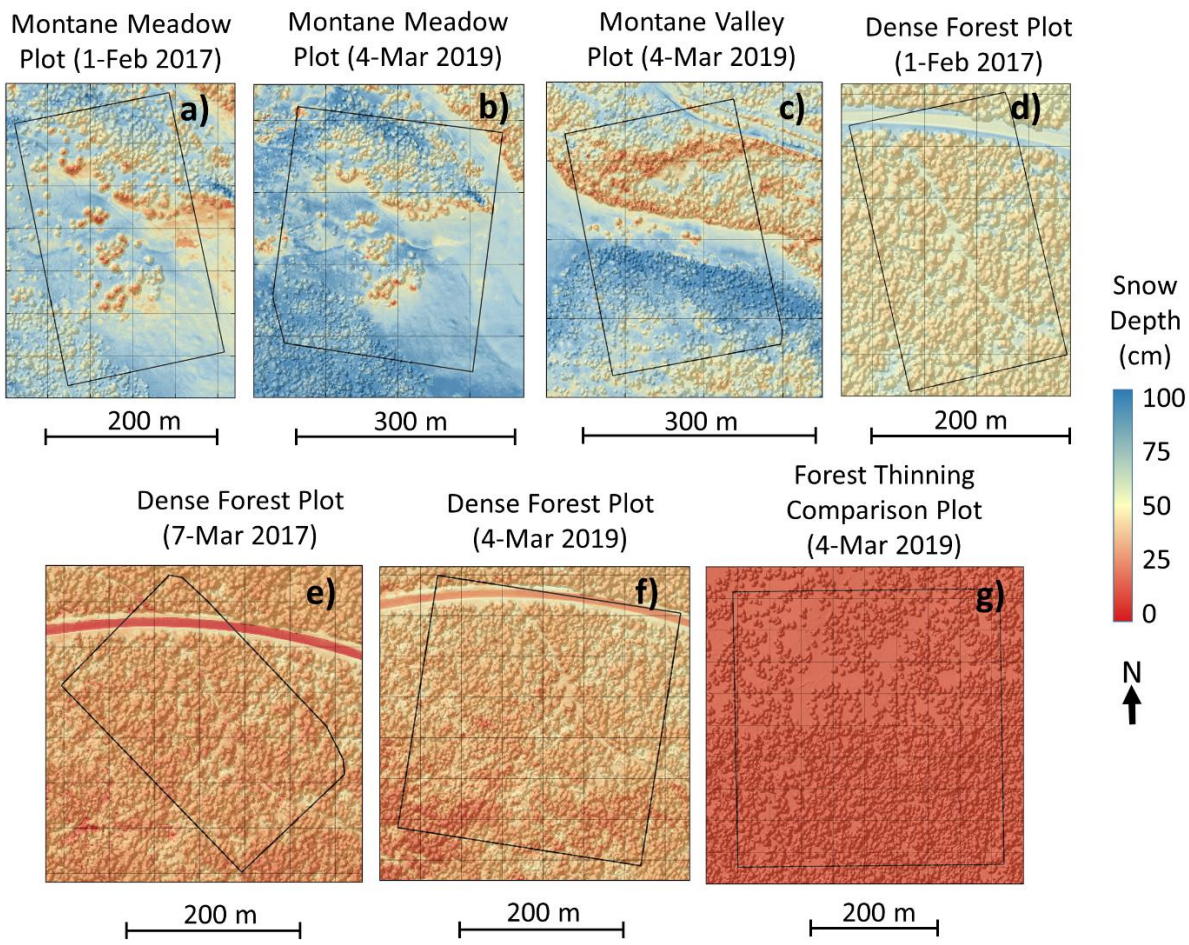

Figure S2. First guess snow depth map generated using the ANN methodology described in section 2.2 for the paired manned aircraft lidar-UAS SfM surveys for the montane meadow plot on 1 February 2017 (**a**) and 4 March 2019 (**b**); the montane valley plot on 4 March 2019 (**c**); the dense forest on 1 February 2017 (**d**), 7 March 2017 (**e**), and 4 March 2019 (**f**); and thinning comparison plot on 4 March 2019 (**g**). A canopy hillshade effect is added to show the locations of trees.

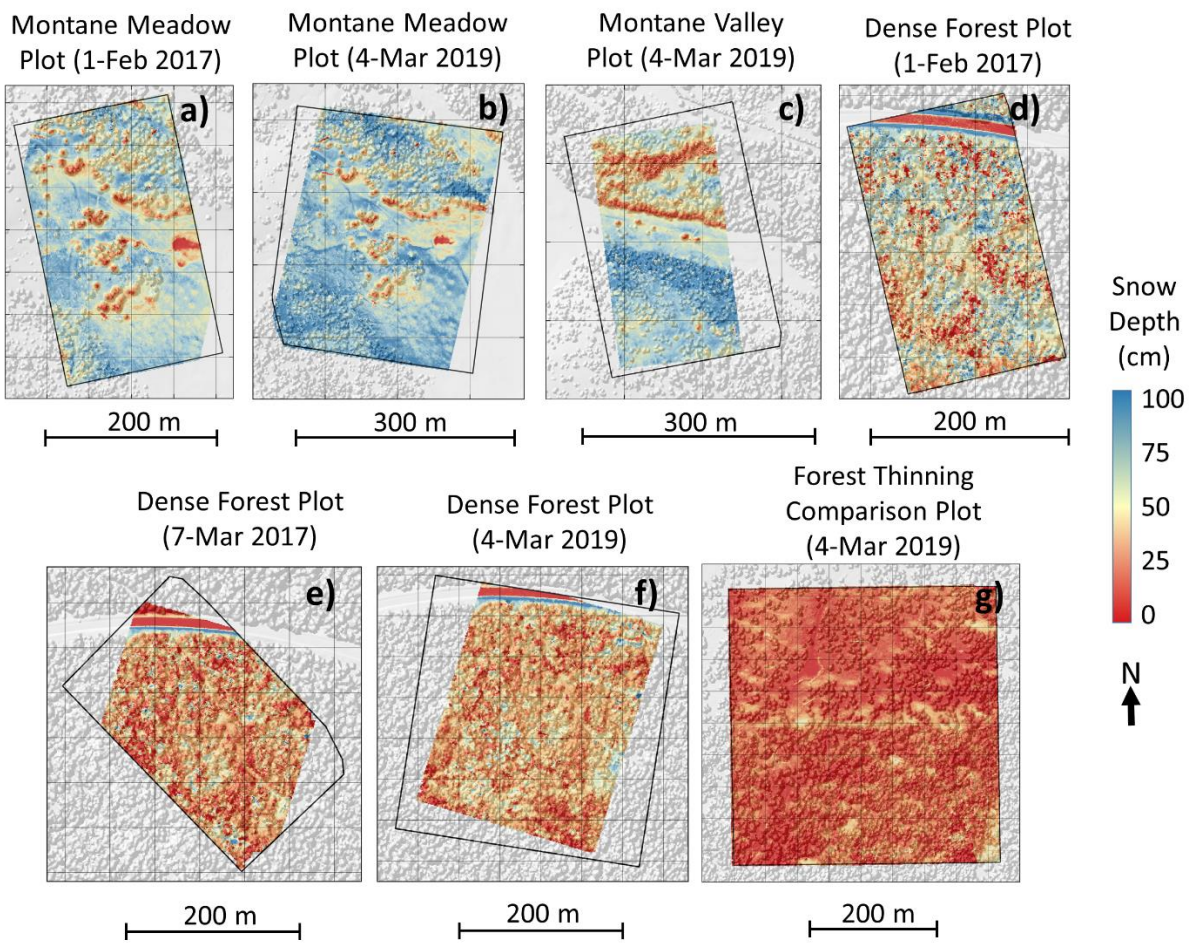

Figure S3. Snow depth maps generated by comparing snow-on vs. snow-off SfM data (vs. those generated by comparing snow-on SfM data and snow-off lidar data in the main manuscript) for the paired manned aircraft lidar-UAS SfM surveys for the montane meadow plot on 1 February 2017 (**a**) and 4 March 2019 (**b**); the montane valley plot on 4 March 2019 (**c**); the dense forest on 1 February 2017 (**d**), 7 March 2017 (**e**), and 4 March 2019 (**f**); and thinning comparison plot on 4 March 2019 (**g**). A canopy hillshade effect is added to show the locations of trees. The black lines show the extents of the coverages in Figure 3. Note that the SfM maps generated with snow-off SfM data are slightly smaller because the snow-on and snow-off surveys did not precisely match.

Table S1. Agreement statistics between lidar and SfM snow depth data (generated by comparing snow-on and snow-off SfM point clouds) shown in Figure S1 (first three columns), and between the lidar snow depth data and first-guess snow depth maps shown in Figure S2 (last three columns). Statistics are for the data within the outlined areas for each plot in Figures S1 and Figure S2.

	Snow Depth First Guess			**Using Snow-Off SfM**		
	R^2	**RMSE (cm)**	**Bias (cm)**	**R^2**	**RMSE (cm)**	**Bias (cm)**
Montane Meadow (1-Feb 2017)	0.64	11.0	-2.8	0.67	11.6	-2.8
Montane Meadow (4-Mar 2019)	0.61	12.6	-3.5	0.67	12.4	-3.5
Montane Valley (4-Mar 2019)	0.80	12.1	-1.5	0.85	10.4	-1.5
Dense Forest (1-Feb 2017)	0.21	15.2	-5.8	0.23	24.0	-6.4
Dense Forest (7-Mar 2017)	0.16	17.9	-5.1	0.22	20.5	-3.7
Dense Forest (4-Mar 2019)	0.25	14.4	-5.5	0.28	17.4	-5.0
Thinning Comparison (4-Mar 2019)	0.07	8.4	0.4	0.40	7.5	1.2

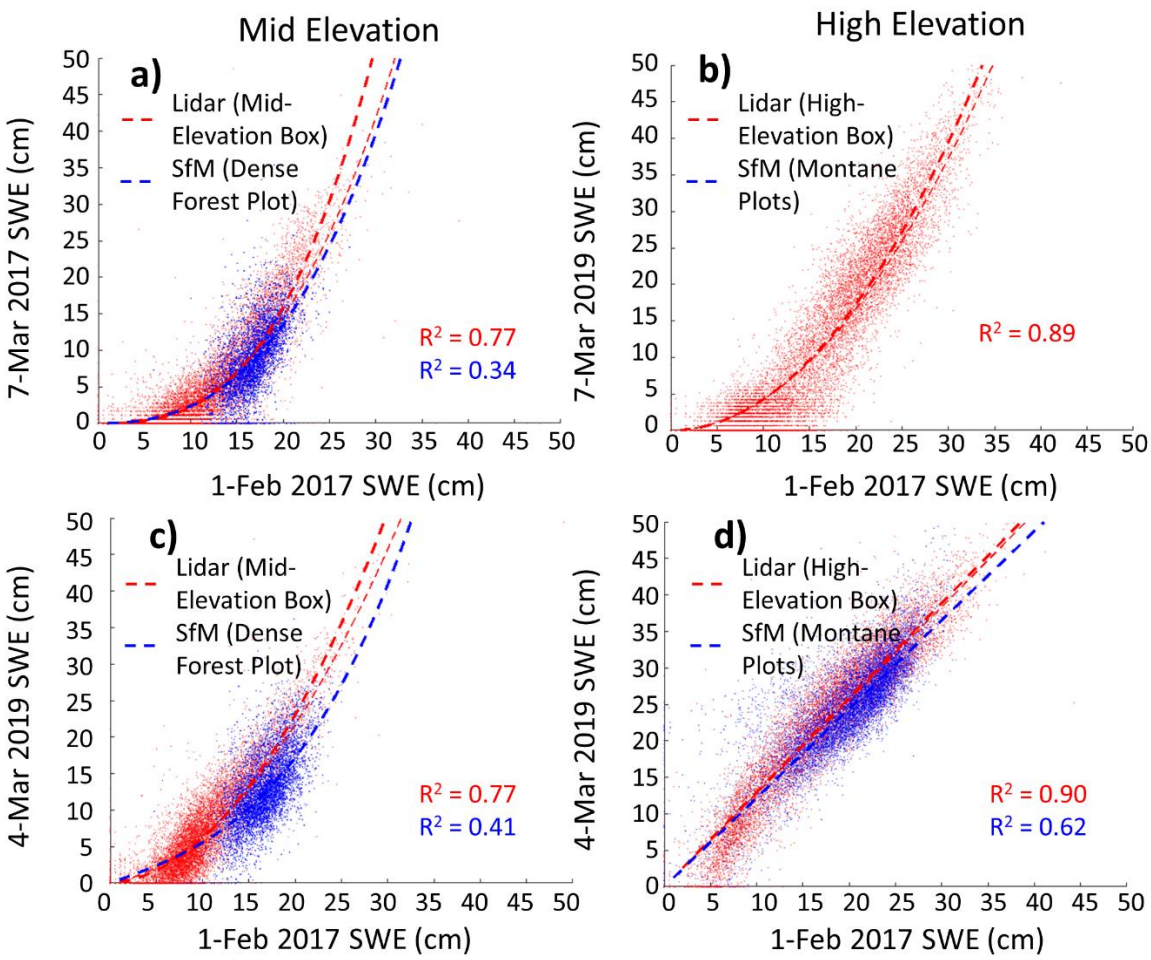

Figure S5: Similar to Figure 5 in the main text. Relationships between 1 February 2017 lidar SWE and 7 March and 4-Mar 2019 lidar (red dots, for the entire lidar coverages) and SfM (blue dots, for the SfM survey plots, based on open pixels) SWE data for the mid-elevation (**a, c**) and high-elevation (**b, d**) lidar coverages. The dashed lines show 3rd order polynomial regressions for each data series (for the lidar regression, additional lines have been added to show the similarity of the comparisons when using only open pixels (thin red dashed lines) and all pixels (thick red dashed lines). The open area SfM regressions (blue lines) are used to simulate the 4-Mar 2019 snow depths for the manned aircraft lidar coverages in Figures S6 and S7.

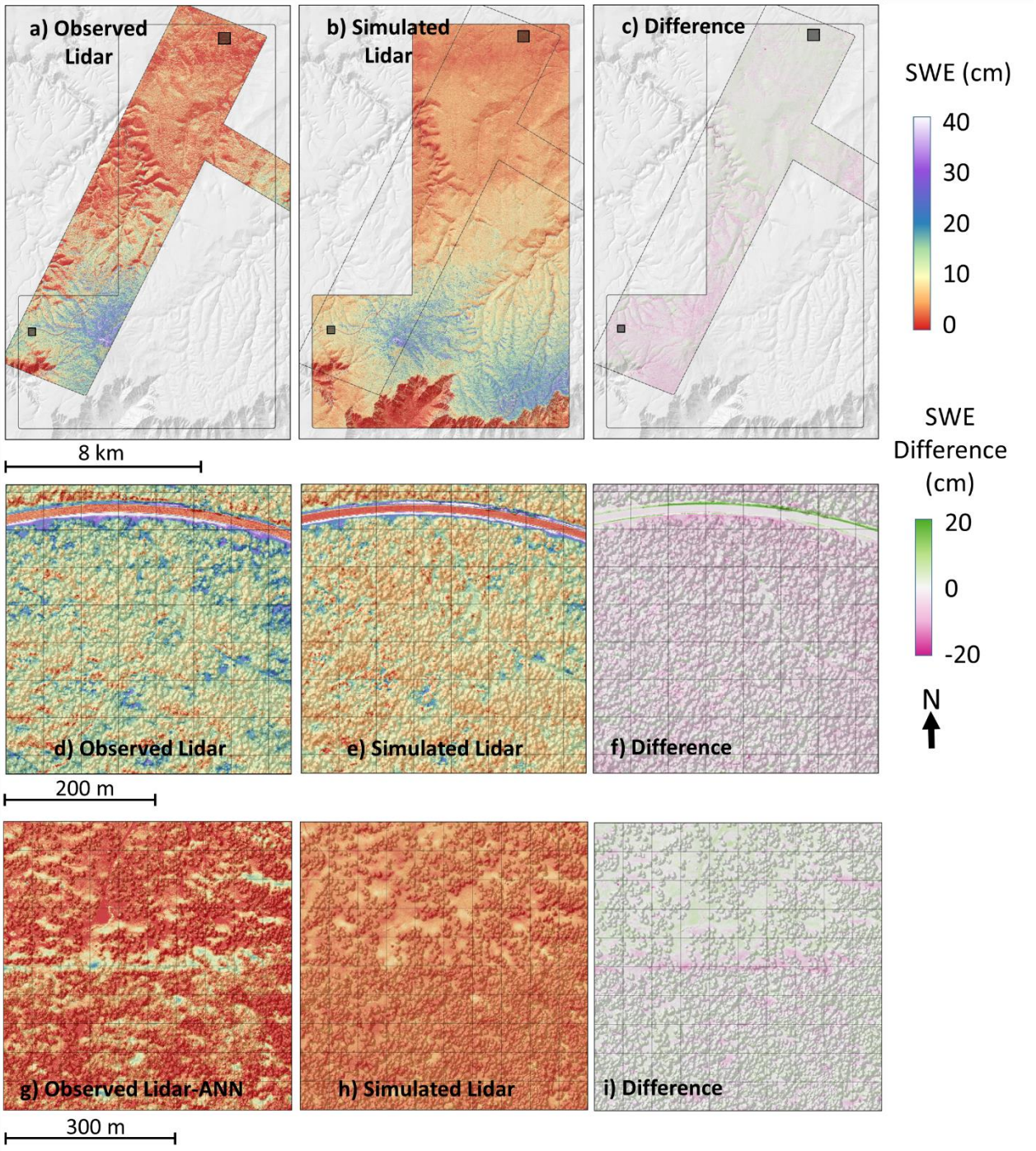

Figure S6. Observed lidar-based SWE map for 4-Mar 2019 SfM data, simulated data (using the regression between the 4 March 2019 SfM data and 1 February 2017 lidar data and shown in Figure S5c), and the difference (simulated-observed) for the mid-elevation lidar coverage (**a–c**) and the area around the dense forest (**d–f**) and thinning-comparison (**g–i**) plots. Note that the simulated SWE values are for the area covered by the 1 Feb. 2017 lidar, while the Mar 2019 lidar has a different footprint. The small dark boxes in (**a–c**) show the area covered by the inset maps (**d–i**) corresponding to the plots in Figure 1.

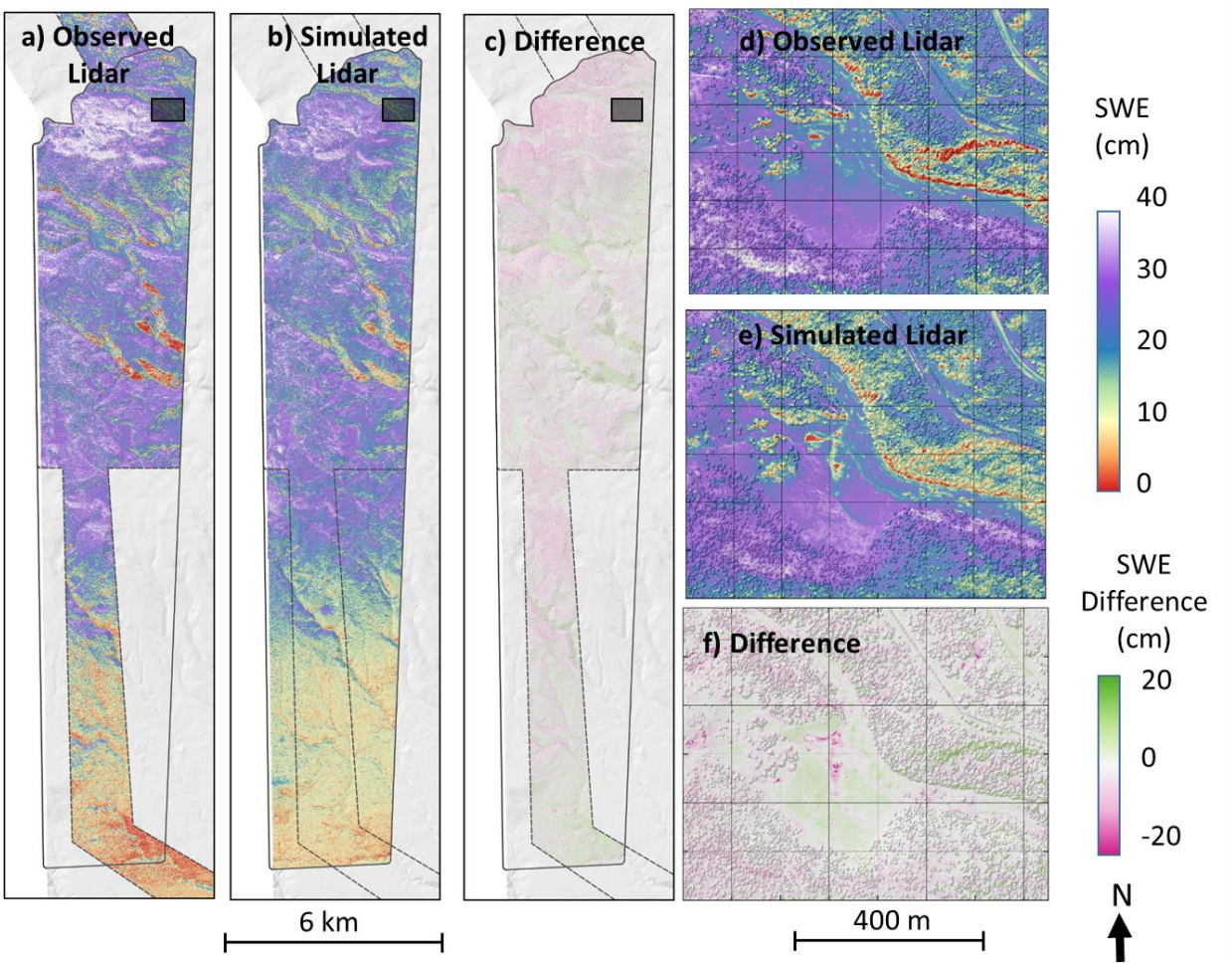

Figure S7. Observed lidar-based SWE maps for 4-Mar 2019, simulated data (using the regression between 4 March 2019 SfM data and 1 February 2017 lidar data shown in Figure 5d), and the difference (simulated-observed) for the high-elevation lidar coverage (**a**–**c**) and the area around the montane plots (**d**–**f**). Note that the simulated SWE values are for the area covered by the 1 Feb. 2017 lidar, while the Mar 2019 lidar has a different footprint. The small dark boxes in (**a**–**c**) show the area covered by the inset maps (**d**–**f**) corresponding to the plots in Figure 1.

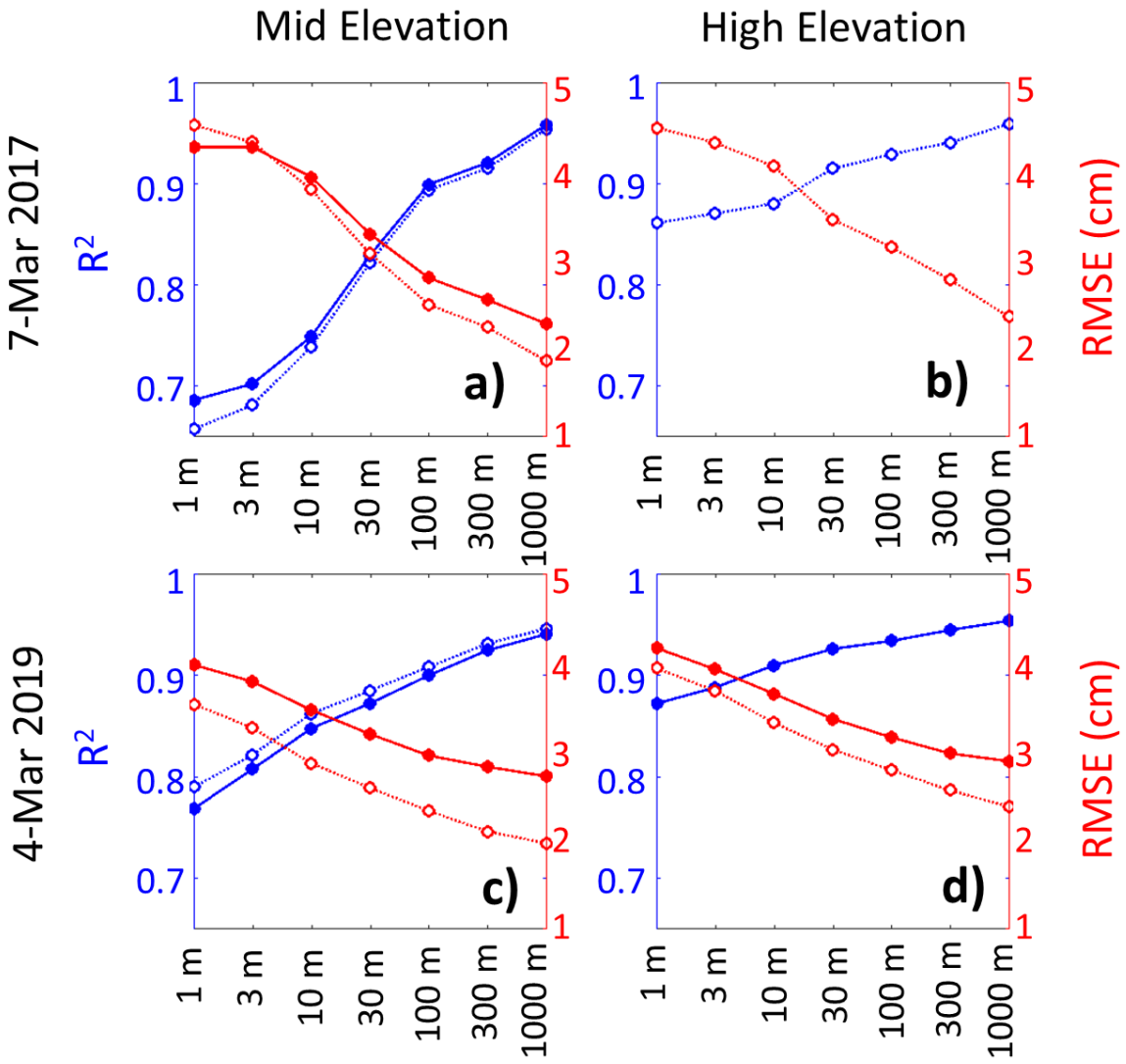

Figure S8. Performance of the simulated SWE maps for the mid- and high-elevation lidar coverages on 7 March 2017 (**a**–**b**) and 4 March 2019 (**c**–**d**) for different pixel scales. The original 1 meter maps are aggregated (by averaging) to the larger pixel scales. The solid lines depict the performance of the simulated maps, created using the relationships between the 1 February 2017 and subsequent SFM data (to assess the actual ability of the SfM data to predict snow depth distributions over the larger lidar domains). The dashed lines depict the performance of the simulated maps, created using the relationships between the 1 February 2017 and subsequent SFM data (to assess the potential ability of the SfM data to predict snow depth distributions over the larger lidar domains).